J Sci Comput (2009) 39: 1–27
DOI 10.1007/s10915-008-9248-y

Subharmonic Resonance Behavior for the Classical Hydrogen Atomic System

Daniel C. Cole · Yi Zou

Received: 11 May 2005 / Revised: 23 August 2008 / Accepted: 23 August 2008 /
Published online: 3 October 2008

Abstract Previously unexplored resonance conditions are shown to exist for the classical hydrogen atomic system, where the electron is treated as a classical charged point particle following the nonrelativistic Lorentz-Dirac equation of motion about a stationary nucleus of opposite charge. For circularly polarized (CP) light directed normal to the orbit, very pronounced subharmonic resonance behavior is shown to occur with a variety of interesting properties. In particular, only if the amplitude of the CP light exceeds a critical value, will the resonance continue without radius and energy decay. A perturbation analysis is carried out to illustrate the main features of the behavior. The present phenomena adds to a growing list of other nonlinear dynamical behaviors of this simple system, that may well be important for more deeply understanding classical and quantum connections.

Keywords Hydrogen · Rydberg · Stochastic · Electrodynamics · Simulation · Classical · Nonlinear

1 Introduction

This article investigates a set of very pronounced subharmonic resonance behaviors for the classical hydrogen atomic system. Other nonlinear behaviors of this system have been discussed in relatively recent articles [1–5]. As described in these articles, this classical hydrogen atom is of interest for several reasons, particularly the following: (1) For large radii, with classical electromagnetic zero-point (ZP) radiation included, then this system should well describe the Rydberg atomic system, with possible distinct advantages in terms of simulation time for modeling its behavior. Such modelling may well be helpful in terms of

D.C. Cole (✉)
Dept. of Manufacturing Engineering, Boston University, 15 St. Mary's Street, Brookline, MA 02446, USA
e-mail: dccole@bu.edu

Y. Zou
One AMD Place, P.O. Box 3453, MS 78, Sunnyvale, CA 94088-3453, USA

engineering manipulations of Rydberg systems, such as for ionization control and chemical reaction control. (2) The mathematical nature of this very nonlinear system exhibits a number of interesting behaviors and forms an interesting test for examining connections between quantum and classical chaotic analyses. (3) This system is of keen interest in the physical theory called stochastic electrodynamics (SED) [6, 7], where it appears that this physical system, combined with the influence of classical electromagnetic zero-point radiation, has a close connection with the predictions of quantum mechanics, at least for the ground state of hydrogen [5]. Much more needs to be investigated regarding the latter to see how far this connection reaches, or ends. However, clearly, the classical electromagnetic radiation spectrum does act to provide a significant stabilizing influence on the otherwise classical problem of collapse for the hydrogen atom. Many of these points are discussed in more detail in [1–5] and so will not be elaborated on much further here.

The present article continues the investigation of some of the interesting nonlinear dynamics of this classical hydrogen system, but focuses on nonlinear subharmonic resonance conditions. To our knowledge, such considerations have not been investigated elsewhere. However, we do note that there are suggestive connections between what is reported here and experimental work [8–10] involving applied microwaves perturbing atomic Rydberg systems, where it has been found experimentally that both ionization and stabilization effects depend on many critical factors. In particular, these factors involve the ratio of the applied microwave signal to the classical Keplerian frequency of the Rydberg orbit, and the strength of the microwave signal. Such effects fall readily out of our classical analysis described here. Our belief is that a full connection between what is reported here, and what is observed experimentally, will in addition require taking into account quantum mechanical effects, possibly by folding in the classical electromagnetic zero-point radiation as done in stochastic electrodynamics [5–7]. Nevertheless, it is certainly gratifying to see that even without such considerations, one qualitatively sees experimental effects such as reported in [10] arise quite naturally in the classical context, as predicted in [1–4].

The trajectory of a classical electron will be treated here via the nonrelativistic Lorentz-Dirac equation [11] of:

$$m\frac{d^2\mathbf{z}}{dt^2} = -e^2\frac{\mathbf{z}}{|\mathbf{z}|^3} + \frac{2e^2}{3c^3}\frac{d^3\mathbf{z}}{dt^3} - e\mathbf{E}[\mathbf{z}(t),t] - \frac{e}{c}\frac{d\mathbf{z}}{dt}\times\mathbf{B}[\mathbf{z}(t),t], \tag{1}$$

where m is the mass of the classical electron, $-e$ is its charge, c is the speed of light, $-e^2\frac{\mathbf{z}}{|\mathbf{z}|^3}$ is the Coulombic binding force, $\frac{2e^2}{3c^3}\frac{d^3\mathbf{z}}{dt^3}$ is the nonrelativistic radiation reaction term, and $\mathbf{E}[\mathbf{z}(t),t]$ and $\mathbf{B}[\mathbf{z}(t),t]$ are electric and magnetic fields acting on the system. When $\mathbf{E}[\mathbf{z}(t),t] = \mathbf{B}[\mathbf{z}(t),t] = 0$, then we have the dilemma noted by physicists after Rutherford's proposed solar system type model of the atom, that each orbit of the electron will slowly, but constantly, keep radiating electromagnetic energy, leading to the collapse of the atom. For an initial circular orbit of 0.5 Å, the time for full decay is about 1.3×10^{-11} s. However, when this classical atom interacts with applied electromagnetic radiation, such as circularly polarized light in the case of an initial circular orbit [1], or an infinite set of plane waves with frequencies that are harmonics of the orbit in the case of an initial elliptical orbit [2], then very dramatic resonance conditions can be achieved that result in a considerable range of nondecaying states for longer period of times, although, in general, decay does eventually set in [3, 4]. Finally, when this system interacts with classical electromagnetic zero-point (ZP) radiation, then not only does a stochastic, but stable, pattern of fluctuating orbits arise, but indications are that the pattern comes close to that predicted by quantum mechanics [4, 5]. It should be noted that this behavior is not unexpected in many ways, since classical

electromagnetic ZP radiation has a number of important properties that have led a relatively small number of researchers to expect the simulated ground state behavior to occur [6]. In particular, classical electromagnetic ZP radiation possesses the natural properties expected of a thermodynamic equilibrium spectrum at temperature $T = 0$, including a form of Lorentz invariance [6, 12] and the property that no heat flows during reversible processes for systems examined in detail to date [7, 13, 14].

What will be examined here is the situation where the classical electron begins in a circular orbit, with a circularly polarized (CP) plane wave propagating normal to the plane of the orbit, similar to what was considered in [1]. However, now instead of considering the CP plane wave with a frequency the same as the initial orbit, here we consider the case where the angular frequency of the CP wave is a factor of n times the orbital frequency. As will be shown, a dramatic resonance-like behavior arises. Although such subharmonic resonance conditions are well known to exist for one dimensional (1D) nonlinear oscillator systems [15], the specific behaviors of this particular 2D nonlinear oscillator-like system are most interesting. Here we bring out some of the main features and relate some of the characteristics to a perturbation analysis.

Undoubtedly most researchers who read this work will find the subharmonic resonance behavior reported here most curious and unusual, since it is likely that the classical hydrogen atom has long been expected to yield little of interest. Clearly, though, such is not the case. Nevertheless, these same researchers may wonder why emphasis has been placed on near circular orbits in [1, 3, 4], and in the present article. Reference [2] did address near elliptical orbits, but even here, the full class of possible orbits is clearly highly restricted.

The reason for these restrictions is simply to gain insight. At present, we do not know how to handle the general orbital case, nor know what to expect in terms of unusual and interesting properties. Analysis of near circular and near elliptical orbits can be carried out. We expect that many of the properties shown here, and elsewhere for near circular orbits, to carry over in a generalized fashion to near-elliptical, just as occurred for [1] and [2]. Still, this remains to be shown, as does the case for yet more general orbits. One needs to start analyzing the system somewhere, which is what the present work attempts to accomplish.

The outline of the article is the following. First, in Sect. 2, we illustrate some of the main features of the subharmonic resonances that we have uncovered by the use of numerical simulation experiments. After displaying a plethora of these general features, we then turn to a perturbation analysis in Sect. 3 that helps to gain some insight into the general behaviors seen in the previous section. Section 4 then turns to a simulation study on the very delicate balance that occurs when the amplitude of the CP plane wave is just sufficiently large to enable a subharmonic resonance condition to take place. Finally, Sect. 5 contains some concluding remarks on this work.

2 Numerical Demonstrations of Subharmonic Nonlinear Resonance Behavior

We now turn to an examination of subharmonic resonances, where the electron begins in an initial circular orbit of radius r_n, $n = 2, 3, \ldots$, with a CP plane wave of an angular frequency that corresponds to the angular frequency of the classical electron if it was to follow a circular orbit of smaller radius, that we will designate as r_1. To make this more clear, we know from classical nonrelativistic mechanics, if a particle of mass m follows a circular orbit of radius r under the sole influence of the Coulombic binding force of $-e^2/r^2$, then from $m\omega^2 r = e^2/r^2$, the angular frequency of this orbit of radius r will be $\omega = (\frac{e^2}{mr^3})^{1/2}$. In

the previous work of [1, 3], and [4], this was the situation examined, where in addition a CP plane wave also acted with this same angular frequency to perturb the motion.

Now we will consider initial circular orbits of radius $r_n > r_1$, where the angular velocity of the circular orbit of radius r_n is

$$\omega_n = \left(\frac{e^2}{mr_n^3}\right)^{1/2} = \frac{\omega_1}{n}, \tag{2}$$

so that $\omega_1 = n\omega_n$. Consequently, from (2), the relation between r_1 and r_n is given by

$$r_n = r_1 n^{2/3}. \tag{3}$$

The relationship of $\omega_1 = n\omega_n$, constitutes the origin of our terminology of "subharmonic" resonance behavior, which corresponds to the terminology used in nonlinear dynamics where very extensive studies have been carried out, particularly for 1D nonlinear oscillators (see, for example, [15]). We will shortly look at a wide variety of instances where the classical electron begins in a circular orbit of radius $r_n = r_1 n^{2/3}$, but with a CP plane wave acting on the orbit, not with the angular frequency ω_n, but with the angular frequency $\omega_1 = n\omega_n$. As in our previous studies, we still confine ourselves to motion of the orbit in a single plane, with nonrelativistic dynamics, and with the CP plane wave directed normal to the plane of the orbit.

Perhaps one of the best ways to first illustrate the dramatic effect of this subharmonic driven motion is to start the electron in a fairly large circular orbit, allow it to decay in its orbit by the usual classical nonrelativistic radiation reaction term of $\frac{2e^2}{3c^3}\frac{d^3\mathbf{z}}{dt^3} = \frac{2e^2}{3c^3}\frac{d}{dt}(\frac{d^2\mathbf{z}}{dt^2}) \approx \frac{2e^2}{3c^3}\frac{d}{dt}(-\frac{e^2\mathbf{z}}{m|\mathbf{z}|^3})$, and the whole time have a CP plane wave acting with angular frequency ω_1.

In the simulations about to be shown, the following equations of motion were used, as written in polar coordinates of r and θ:

$$\ddot{r} - r\dot{\theta}^2 = -\frac{e^2}{mr^2} + \frac{2\tau e^2}{m}\frac{\dot{r}}{r^3} + \frac{eA}{m}\sin(\theta - \omega_1 t - \alpha), \tag{4}$$

and

$$r\ddot{\theta} + 2\dot{r}\dot{\theta} = -\frac{\tau e^2}{m}\frac{\dot{\theta}}{r^2} + \frac{eA}{m}\cos(\theta - \omega_1 t - \alpha), \tag{5}$$

where α is a phase factor between the initial electric field direction of the CP plane wave and the velocity direction of the classical electron (see, for example, Fig. 1 in [4]). Equations (4) and (5) come from (1), (i) as written in polar coordinates, (ii) with the approximation just mentioned for the radiation reaction, and (iii) with the neglect of the magnetic Lorentz force term, $-\frac{e}{c}\frac{d\mathbf{z}}{dt} \times \mathbf{B}[\mathbf{z}(t), t]$. This term acts to push the particle out of the plane, but its magnitude is small due to $|\dot{\mathbf{z}}/c| \ll 1$ for the cases examined, so this term only becomes important if the time of simulation becomes appreciable. In several cases, the simulations reported were run with and without this term, and for these cases little effect was noticed. Consequently, to ease analytic understanding of the key subharmonic resonance effect, the magnetic Lorentz force term was not included in subsequent reported simulations and analysis.

The means for numerically solving (4) and (5) were carried out using an adaptive stepsize fifth-order Runge–Kutta routine [16]. These equations of motion are quite nonlinear, first due to the Coulombic binding force, but also due to the Lorentz force from the plane waves and the electromagnetic damping term. The algorithm permits an initial setting on numerical accuracy of each time step. However, given any initial precision chosen, the simulations

eventually breaks down if carried out far enough in time. To go out farther in time requires yet higher precision, with substantially growing times in computation (CPU). Such behavior is of course typical of most strongly nonlinear system. For the simulations reported here, several runs of increasing precision were typically run to ensure that what was reported, for the time period shown, was indeed accurate.

When $r = r_n$, and with $\omega_n = (\frac{e^2}{mr_n^3})^{1/2}$, then the first term on the right in (4) becomes

$$\frac{e^2}{m(r_n)^2} = \omega_n^2 r_n,$$

with $\omega_n = \frac{\omega_1}{n}$, which is the main source of the subharmonic resonance behavior we will be examining.

In Fig. 1(a), the classical electron was started in a circular orbit of 2 Å, with a CP plane wave acting with a much higher angular frequency, that corresponds to an electron going in a circular orbit of radius 0.5 Å. Figure 1(a) shows radius, r, versus time, t, for a set of numerical experiments where the classical electron was in each case started at $r = 2$ Å, but where CP plane waves of different amplitudes were acting, ranging, as shown, from 10 to 5000 statvolt/cm. When resonance occurred, which happened for values of 100 statvolt/cm $\lesssim A$, the envelope of the r vs. t curves became very similar, with only the details of the behavior inside the envelope changing substantially, and with the time to decay also varying depending on the value of A. The horizontal line labelled as r_2 has the numerical value here of 0.5 Å $\times 2^{2/3} = 0.7937$ Å. As can be seen, the envelope of the resonance curves are roughly centered around this value. Figure 1(b) zooms in on the two curves for $A = 10$ and $A = 50$ statvolt/cm. Prior to decaying to the $r_2 = 0.7937$ Å value, these two curves are very similar; after that, a slight resonance can be seen to begin for the $A = 50$ statvolt/cm case, which is superimposed over the much thinner $A = 10$ statvolt/cm curve.

Thus, if the amplitude of the applied CP wave is too small, such as 10 or 50 statvolt/cm, then the orbital decay occurs fairly similarly to what happens if no CP plane acts on the electron [1]. Of course, there are small differences in these curves even for such small CP amplitudes, particularly when the decaying orbit reaches r_2, as illustrated in Fig. 1(b). However, the differences in these curves are enormously small compared to what happens in the resonance situations. Note the difference in the vertical scales for Figs. 1(a) and 1(b).

When $A \gtrsim 100$ statvolt/cm for this particular example, then large changes occur when the decaying orbit reaches the r_2 radius. First, a significant delay in decay occurs. Second, the envelope of the oscillations of r vs. t undergoes a dramatic change, with the radius centered roughly around $r_2 = 0.5 \times 2^{2/3}$ Å ≈ 0.7937 Å , but varying within an envelope from about 1.24 Å to 0.36 Å. What is also most interesting is that once a threshold value of A is exceeded, then the ensuing wide envelope curves become very similar, as can be seen in Fig. 1(a), whether one uses $A = 100,\ 500,\ 1000$, or 5000 statvolt/cm. As will be noted shortly, however, the inner details of the behavior between these envelopes is certainly different. However, from just looking at Fig. 1(a), the main obvious distinction between these curves is the time at which the resonance envelope curve is "broken" and orbital decay eventually takes place. Moreover, if A is increased a great deal, as in Fig. 1(c), then we see a transition from orbital decay to one of "ionization," occurring here when $A = 100{,}000$ statvolt/cm. As can be seen, what is most curious is that as A increases, the time to decay initially becomes longer and longer ($A = 10 \rightarrow 500$ statvolt/cm), then decreases ($500 \rightarrow 10{,}000$ statvolt/cm), then increases again ($10{,}000 \rightarrow 50{,}000$ statvolt/cm). Some indications of the peculiarities of these behaviors of resonance and decay can be seen in previous work for the $\omega/1$ resonance case, such as [2, 4], although previously we have

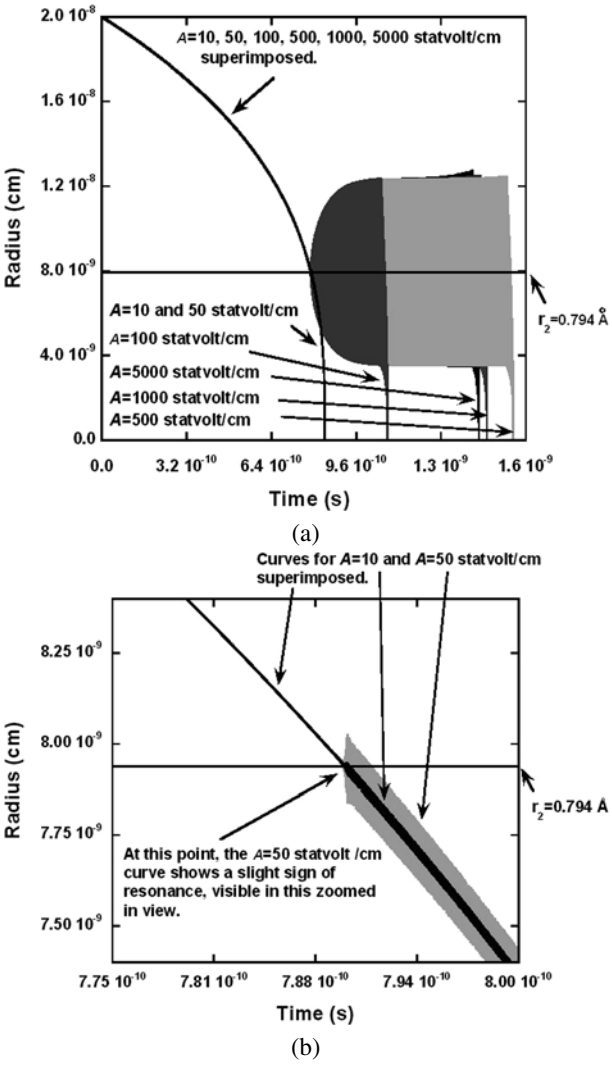

Fig. 1 (**a**) r vs. t for six numerical simulation conditions are shown here, namely, with $A = 10$, 50, 100, 500, 1000, and 5000 statvolt/cm, all with $\alpha = 0$ and $\omega_1 = e/(mr_1^3)^{1/2} \approx 4.50 \times 10^{16}$ s^{-1} in (4) and (5), with $r_1 = 0.5$ Å. In each case, the classical electron began in a circular orbit at $r = 2$ Å. Upon decaying in orbit, strong examples of resonance occurred for $A \gtrsim 100$ statvolt/cm when the decaying radius reached near $r_2 = r_1 \times 2^{2/3} \approx 0.7937$ Å. The envelopes of the curves are remarkably similar, with the most obvious distinction being the times at which orbital decay again sets in. (**b**) Here (**a**) is focused in on for the two curves of $A = 10$ and $A = 50$ statvolt/cm to show that even for $A = 50$ statvolt/cm, there is a slight sign of resonance near $r_2 = 0.7937$ Å value, although not enough to delay the time of orbital decay. (**c**) Here nine simulation conditions are shown, all with the electron starting in a circular orbit at $r = 0.7937$ Å. The amplitude A is increased up to 100,000 statvolt/cm, enough to change the envelope of the curve more substantially and to lead to an ionization-like effect, rather than orbital decay

not published results going to high enough values of A where ionization could set in, nor examined the $\omega/2$ subharmonic resonance case. Upon increasing up to 100,000 statvolt/cm in Fig. 1(c), an ionization effect can be seen. It should be noted that although 100,000 statvolt/cm is certainly very large, the magnitude of the Coulombic electric field at $r = 0.5$ Å is $e/r^2 \approx 1.92 \times 10^7$ statvolt/cm, which is still 192 times larger than the applied field in this numerical experiment.

If one probes the inner details of the r vs. t behaviors, rather than looking only at envelopes of the curves and the points at which either orbital decay or ionization sets in, then additional complex and interesting characteristics appear that look much like "beat" phenomena in the fluctuating orbital quantities. For example, if we consider Fig. 1, and this time do not "drop" the electron from a higher radius, but instead simply start the electron at the r_2 point, and if we zoom in further on the time scale to see more of the details of the r vs. t behavior for different values of A, then plots as shown in Figs. 2(a) and 2(b)

Fig. 1 (*Continued*)

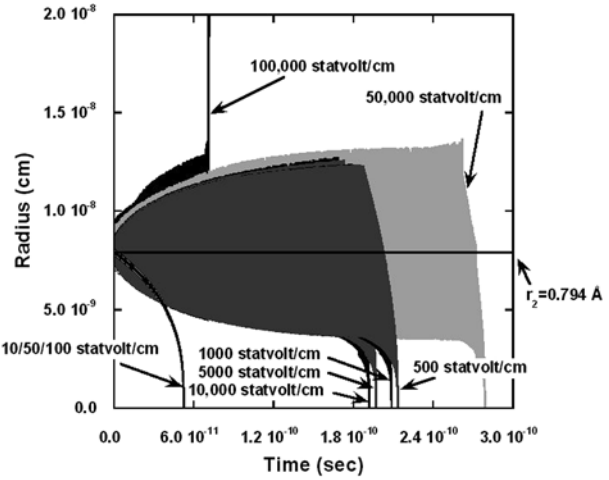

(c)

result. These figures show how the envelopes that appear in Fig. 1(a) are actually composed of many smaller envelopes, that form "beat-like" patterns. Upon focusing in further in either of Figs. 2(a) or 2(b), we see the result shown in Fig. 2(c), that compares the early time evolution of Figs. 2(a) and 2(b). In Fig. 2(c), the radius first starts in a near circular orbit, but then begins spiralling in and out. We will analyze this behavior in some detail in the next section using a perturbation analysis. The peaks and valleys of the curves in Fig. 2(a) and 2(b) superimpose to form the grosser envelope curve shown in Fig. 1(a), with only slight differences in the overall outer envelopes. As A increases, the time distance between these peaks of valleys, of this apparent "beat-like" behavior, become closer and closer together.

Similarly, the higher order ω/n resonance conditions exhibit a plethora of interesting "beat-like" behaviors, as illustrated below in Fig. 3(a) for the $\omega/3$ situation ($r_1 = 0.5$ Å and $r_3 = r_1 \times 3^{2/3} = 1.040$ Å), and in Fig. 3(b) for the $\omega/4$ ($r_4 = r_1 \times 4^{2/3} = 1.260$ Å) case for several values of A large enough to cause the respective $\omega/3$ and $\omega/4$ resonance conditions. Figure 3(c) shows the early time evolution for the $\omega/3$ case in Fig. 3(a), while Fig. 3(b) shows the early time evolution for the $\omega/4$ case. The three curves in Figs. 3(c) and 3(d) are very close in character at the zoomed in early time regions, having only a very slight wiggle (note the y-axis dimensions). In Fig. 3(d), the three curves are essentially indistinguishable. What is also quite remarkable, is the very sharp turn-on characteristic for many of these resonance-like behaviors. This can be seen quite clearly in Fig. 3(e), where just a slight change in the value of A leads to a much longer sustained resonance effect. As seen in Figs. 3(c) and 3(e), the radius at the $\omega/3$ resonance point initially decreases, before curving back up for the $A = 11{,}977$ statvolt/cm case with the envelope greatly widening, while the center of the $A = 11{,}976$ statvolt/cm case continues to decrease in value. Increasing the value of A yet further for the $\omega/3$ leads to ionization like effects, as seen in Fig. 3(f) for the $\omega/3$. The envelopes of the curves behave in a similar manner to the $\omega/2$ subharmonic resonance condition already discussed, where the outer envelopes change somewhat, but not too dramatically as A changes, but the time to orbital decay and/or ionization is very sensitively dependent on the value of A.

It should be noted that the time between peaks in the most detailed of these curves, namely, Figs. 3(c) and 3(d), represent the time for each orbit, namely, $\frac{2\pi}{\omega_3} \approx \frac{2\pi\times 3}{4.5\times 10^{16}} \approx 4.19 \times 10^{-16}$ s, and $\frac{2\pi}{\omega_4} \approx \frac{2\pi\times 4}{4.5\times 10^{16}} \approx 5.59 \times 10^{-16}$ s, respectively. In Sect. 4, we show this in more

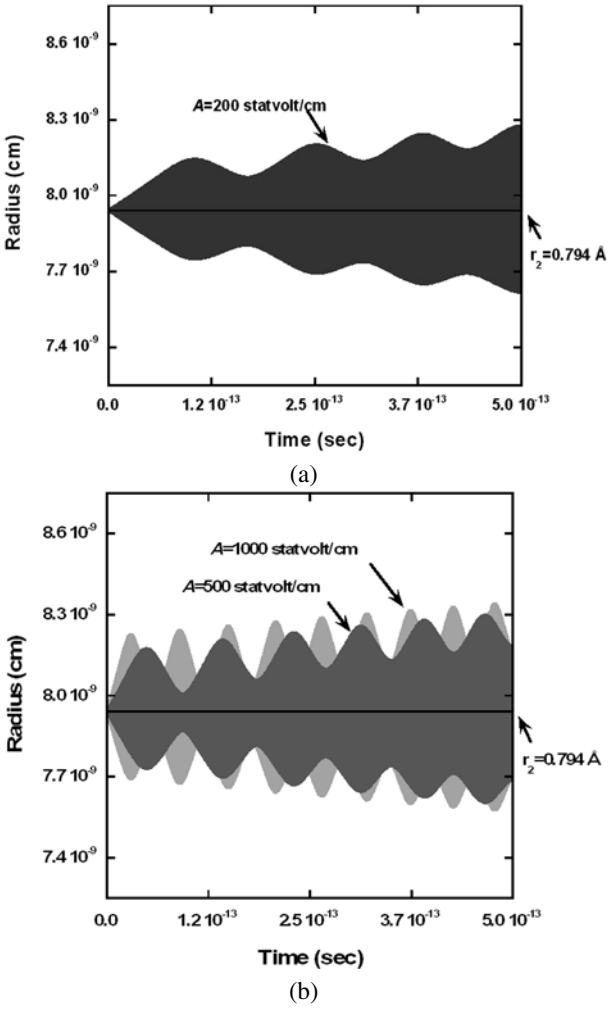

Fig. 2 (**a**) r vs. t when $A = 200$ statvolt/cm and the classical electron begins a circular orbit at $r_2 = r_1 \times 2^{2/3} \approx 0.7937$ Å. As in Fig. 1, $\alpha = 0$ and $\omega_1 = e/(mr_1^3)^{1/2}$ in (4) and (5), with $r_1 = 0.5$ Å. (**b**) Similar trajectories are shown here when $A = 500$ and 1000 statvolt/cm. As A increases, the time difference between the peaks and valleys of the envelope curve become closer together. At the grosser scale of Fig. 1, the envelopes shown here appear to merge. (**c**) Here, the three curves in (**a**) and (**b**) are focused in on to show the finer detail. The time between peaks is roughly the period of a nearly circular orbit at the radius of 0.7937 Å, namely, $\frac{2\pi}{\omega_2} \approx \frac{2\pi \times 2}{4.5 \times 10^{16}} \approx 2.79 \times 10^{-16}$ s

detail by emphasizing the energy versus time curves, that help to show greater insight into the resonance.

In Figs. 3(a)–(g), the value of $r_1 = 0.5$ Å was used, which translated into resonance conditions at $\omega_3 = \frac{\omega_1}{3}$, $r_3 = r_1 \times 3^{2/3} = 1.040$ Å, and $\omega_4 = \frac{\omega_1}{4}$, $r_4 = r_1 \times 4^{2/3} = 1.260$ Å. Thus, increasingly higher values of A are required to make these resonances occur for the $n = 1$ case ($A_{\text{crit}} \approx 5.4$ statvolt/cm), $n = 2$ case ($A_{\text{crit}} \approx 105.7$ statvolt/cm), $n = 3$ case ($A \approx$ 11,977 statvolt/cm), and $n = 4$ case ($A_{\text{crit}} \approx 147{,}120$ statvolt/cm), as seen in the histogram of these values in Fig. 4(a).

In contrast, if we look only at a single resonance condition, such as the $\omega/2$ case, and look at different values of r_2 versus the critical value of A_c where resonance sets in, we obtain a plot as shown in Fig. 4(b). Here, as the radius is increased at which the $\omega/2$ resonance occurs, the critical value of A needed to ensure resonance decreases in value. Figure 4(c) plots r vs. t for the first four of these points, and Fig. 4(d) shows an enlarged view of r vs. t for the first two of these resonant conditions. The center lines indicated in Figs. 4(c)

Fig. 2 (*Continued*)

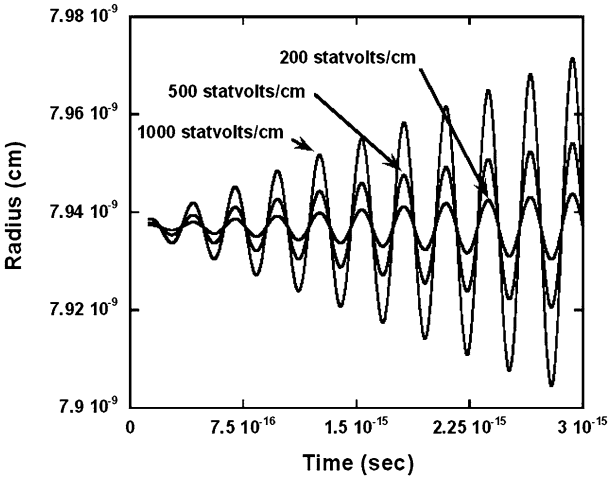

(c)

and 4(d) are the values of r_2 corresponding to the values of r_2 in Fig. 4(b). Finally, Fig. 4(e) plots the data in Fig. 4(b) as $\log_{10}(A_c)$ vs. $\log_{10}(r_2)$, and compares the data versus a curve with $(r_2)^{-7/2}$ dependence. As can be seen, there is a fairly close correspondence over the regime examined.

The reason for expecting a $(r_2)^{-7/2}$ dependence can be understood from (1). If we let $\mathbf{z} = l_0\mathbf{z}'$, and $t = t_0 t'$, so that $\mathbf{z}'$ and t' are dimensionless, then (1) becomes, with $\mathbf{z}$ constrained to a plane perpendicular to the direction of propagation of the CP wave, and, with $\mathbf{E} = A\mathbf{E}'$, where A is the amplitude of the CP wave we have used in our simulations:

$$\frac{ml_0}{t_0^2}\frac{d^2\mathbf{z}'}{dt'^2} = -\frac{e^2}{l_0^2}\frac{\mathbf{z}'}{|\mathbf{z}'|^3} + \frac{m\tau l_0}{t_0^3}\frac{d^3\mathbf{z}'}{dt'^3} - eA\mathbf{E}'. \tag{6}$$

Dividing by $\frac{ml_0}{t_0^2}$ yields:

$$\frac{d^2\mathbf{z}'}{dt'^2} = -\frac{e^2 t_0^2}{ml_0^3}\frac{\mathbf{z}'}{|\mathbf{z}'|^3} + \frac{\tau}{t_0}\frac{d^3\mathbf{z}'}{dt'^3} - \frac{eAt_0^2}{ml_o}\mathbf{E}'. \tag{7}$$

For Figs. 4(b) and 4(e), the natural choice to make for l_0 is $l_0 = r_2$, and for t_0 the natural choice is the period of the orbit, or $t_0 = \frac{2\pi}{\omega_2} = 2\pi(\frac{mr_2^3}{e^2})^{1/2}$. Equation (7) then becomes:

$$\frac{d^2\mathbf{z}'}{dt'^2} = -(2\pi)^2\frac{\mathbf{z}'}{|\mathbf{z}'|^3} + \frac{\tau}{t_0}\frac{d^3\mathbf{z}'}{dt'^3} - \frac{eAt_0^2}{mr_2}\mathbf{E}'. \tag{8}$$

The two largest contributing terms (left side and first on right side) now appear independent of the value of r_2. The other two terms do not scale as nicely. Ideally what we would like is to be able to take an analytic expression for $\mathbf{z}'(t)$ and solve for when A_c occurs to cause resonance. The next section discusses a perturbation expression that works for several hundred orbits, but not for the length of time required, as seen best in Fig. 7(a). Still, we can obtain a rough estimate of the behavior by expecting that at the critical value of A_c for resonance to take place, that the ratio of the two remaining terms should be approximately the same,

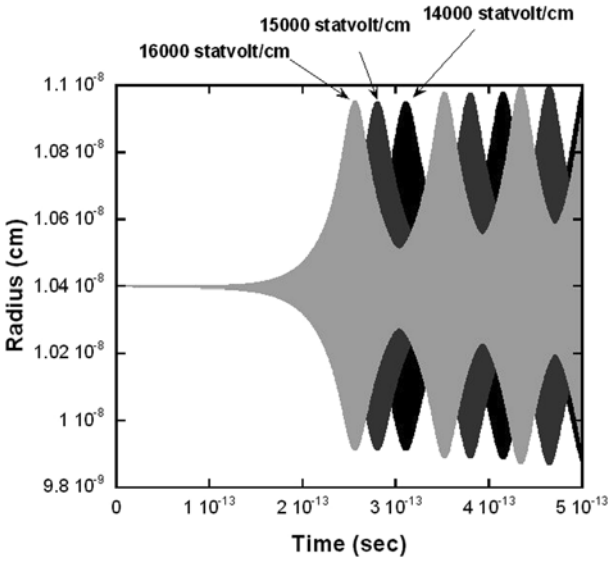

(a)

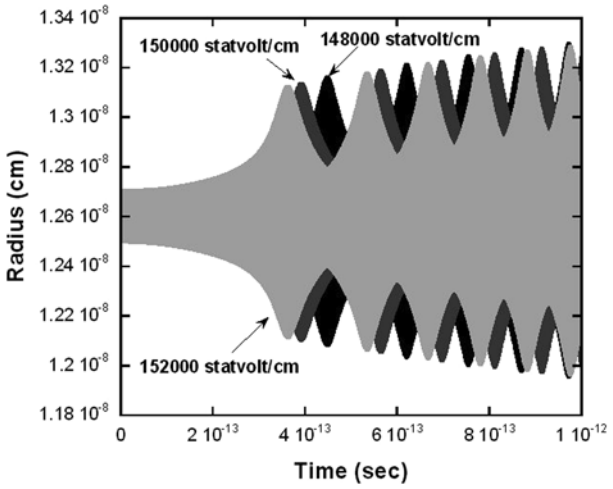

(b)

Fig. 3 (**a**) r vs. t when $A = 14,000$, 15,000, and 16,000 statvolt/cm, and the classical electron begins a circular orbit at the $\omega/3$ subharmonic resonance point of $r_3 = r_1 \times 3^{2/3} \approx 1.040$ Å. The conditions of $\alpha = 0$ and $\omega_1 = e/(mr_1^3)^{1/2}$, with $r_1 = 0.5$ Å in (4) and (5) were used. (**b**) r vs. t when $A = 148,000$, 150,000, and 152,000 statvolt/cm, and the classical electron begins a circular orbit at the $\omega/4$ subharmonic resonance point of $r_4 = r_1 \times 3^{2/3} \approx 1.260$ Å, when $\alpha = 0$, $\omega_1 = e/(mr_1^3)^{1/2}$, and $r_1 = 0.5$ Å in (4) and (5) were used. (**c**) Figure (**a**) is focused in on at the early time period. The distance between peaks is roughly the period of a circular orbit at $r_3 = 1.040$ Å, namely, $\frac{2\pi}{\omega_3} \approx \frac{2\pi \times 3}{4.5 \times 10^{16}} \approx 4.89 \times 10^{-16}$ s. (**d**) Figure (**b**) is zoomed in on at the early time period. The distance between peaks is roughly the period of a circular orbit at $r_4 = 1.260$ Å, namely, $\frac{2\pi}{\omega_4} \approx \frac{2\pi \times 4}{4.5 \times 10^{16}} \approx 5.59 \times 10^{-16}$ s. The three curves are nearly indistinguishable in this plot. (**e**) r vs. t is shown for two very slightly different conditions, $A = 11,976$ and $A = 11,977$ statvolt/cm, for the $\omega/3$ subharmonic resonance condition, where the classical electron starts in a circular orbit at $r_3 \approx 1.040$ Å, with $\alpha = 0$, $\omega_1 = e/(mr_1^3)^{1/2}$, and $r_1 = 0.5$ Å. With only a very small relative change in A, a very considerable change in resonant behavior results. (**f**) r vs. t for the same $\omega/3$ case as in (**a**), (**c**), and (**e**), but now A is increased large enough for ionization effects to occur

Fig. 3 (*Continued*)

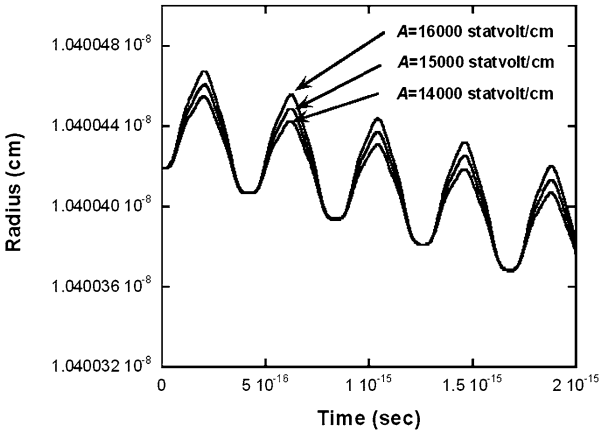

(c)

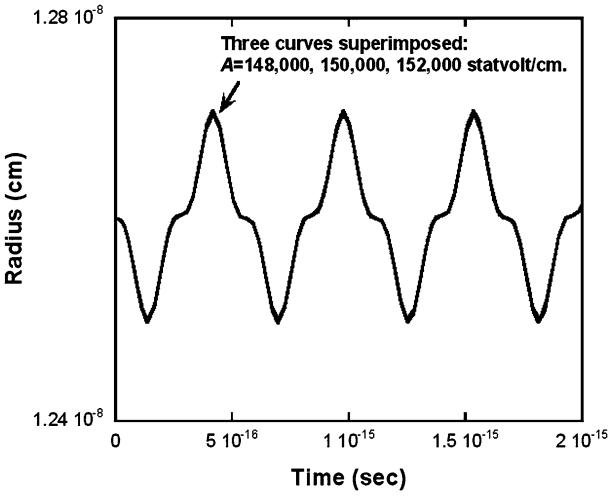

(d)

independent of the value of r_2, or,

$$\frac{(\frac{eA_c t_0^2}{mr_2})}{(\frac{\tau}{t_0})} = k, \tag{9}$$

where k is a constant. Hence:

$$A_c = k\frac{\tau m}{e}\frac{r_2}{t_0^3} = k\frac{\tau m}{e}\frac{1}{(2\pi)^3}r_2\left(\frac{e^2}{mr_2^3}\right)^{3/2} = k\frac{\tau e^2}{(2\pi)^3 m^{1/2}}(r_2)^{-7/2}. \tag{10}$$

In this way, we see how the $(r_2)^{-7/2}$ dependence arises in a natural way in Fig. 4(e).

Fig. 3 (*Continued*)

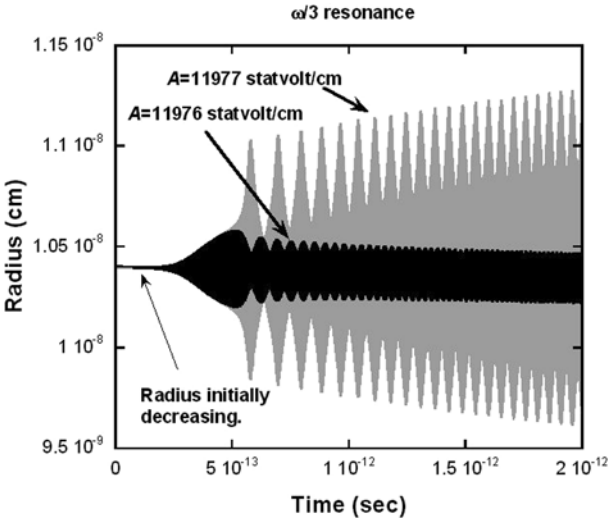

(e)

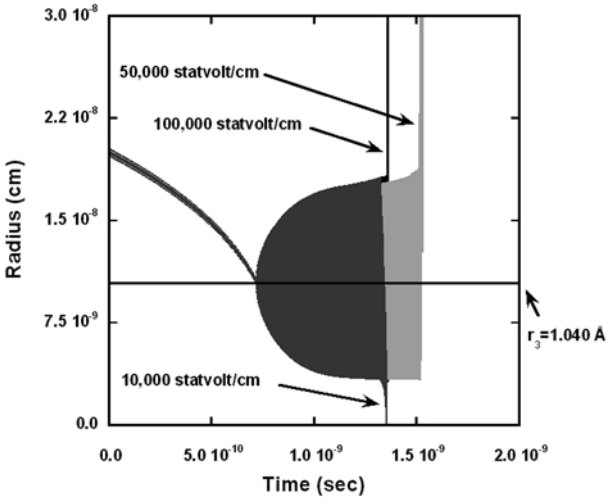

(f)

3 Perturbation Analysis on Subharmonic Resonance

Having now seen a wide variety of interesting nonlinear subharmonic resonance behaviors for the simple classical hydrogen atom, we now turn to a more detailed perturbation analysis to attempt to gain some understanding regarding the origin of these strong resonances. There are a number of excellent sources for perturbation analysis for nonlinear oscillatory systems, particularly for 1D oscillators, as in [15] and the references cited therein. The 2D nature of the present system, due to (4) and (5), make the analysis more difficult, however. The present system somewhat resembles a Duffing oscillator, in that there is a forcing term and a damping term; one problem is that as the orbit changes a lot, the higher order corrections to the binding potential become quite key. Several perturbation methods are available to use, such as the method of multiple scales and the Linstedt-Poincaré method, both of which are

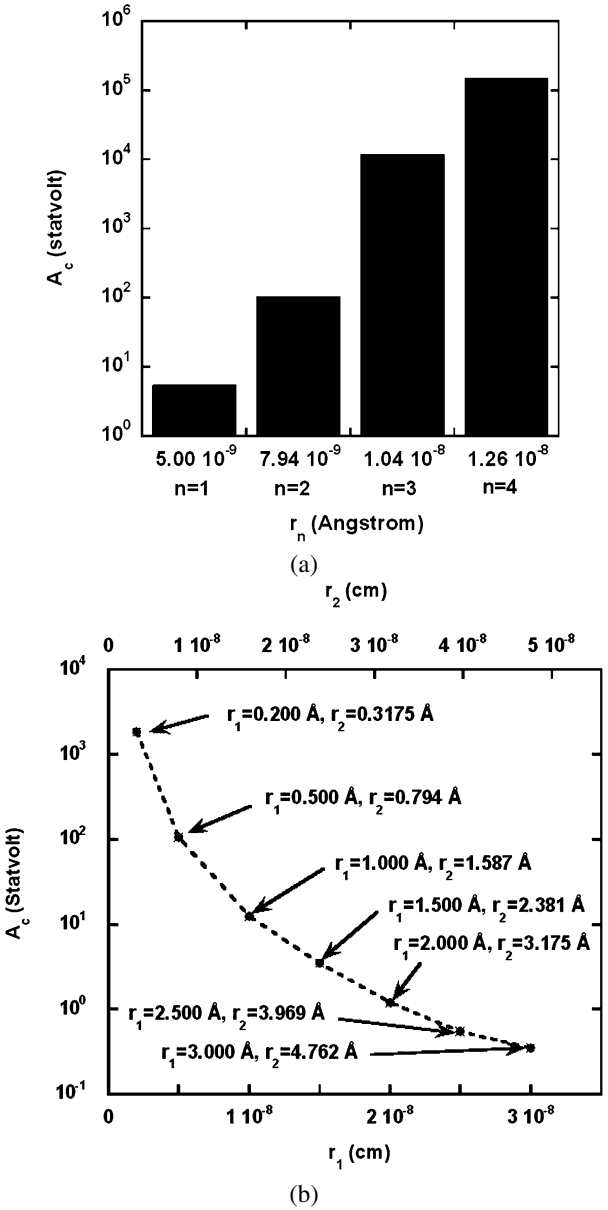

Fig. 4 (**a**) A histogram is shown of the values of A_{crit} needed to obtain the resonance points of $n = 1, 2, 3$, and 4. In each case, $\alpha = 0$, $r_1 = 0.5$ Å, and the particle was started in a circular orbit at the respective radii of r_1, $r_2 = r_1 2^{2/3}$, $r_3 = r_1 3^{2/3}$, and $r_4 = r_1 4^{2/3}$, using (4) and (5). (**b**) Here, different values of r_2 and r_1 are plotted versus the critical value of A needed to establish an $\omega/2$ resonance condition. More specifically, at each point $r_2 = r_1 \times 2^{2/3}$. Each point represents a different numerical simulation at a different initial circular orbit, r_2, with a CP plane wave acting with $\alpha = 0$, the indicated value of A_c needed to establish an $\omega/2$ subharmonic resonance condition, and with $\omega_1 = e/(mr_1^3)^{1/2}$. As r_1 and r_2 increase, the value of A_c needed to establish resonance decreases as shown. (**c**) r vs. t for the first four $\omega/2$ resonance conditions in (**b**). (**d**) A blown up plot of r vs. t for the first two $\omega/2$ resonance conditions in (**c**). (**e**) The values of A_c vs. r_2 are plotted here in a log-log plot. From (10), we expect that $\log_{10}(A_c) = \log_{10}(k\frac{\tau e^2}{(2\pi)^3 m^{1/2}}) - \frac{7}{2}\log_{10}(r_2)$. As can be seen from the *dashed line*, this curve has a fairly close correspondence to the simulated data

well documented for 1D oscillators. For 2D oscillators, the identification of the appropriate expansion parameters certainly becomes more problematic.

Consequently, in the present work we will use the simplest expansion method, which at least gets to the heart of the issues very quickly, enables the initial trajectory to be easily modelled, and quickly reveals the origin of the resonance behaviors. In some ways this is perhaps preferable, since many of the long term behaviors shown in the previous section would truly require fairly heroic expansion methods to obtain such long term agreement with

Fig. 4 (*Continued*)

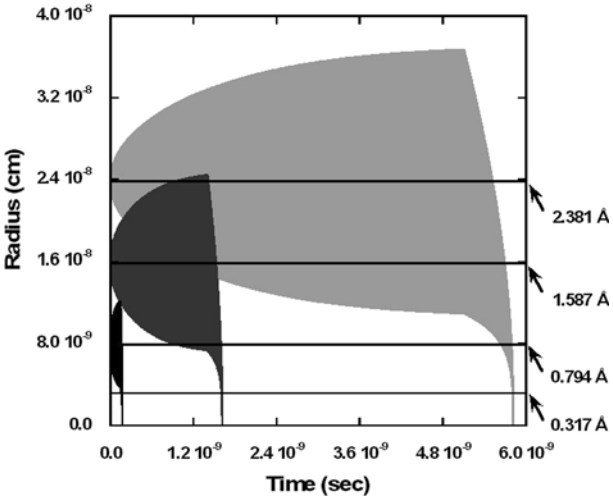

(c)

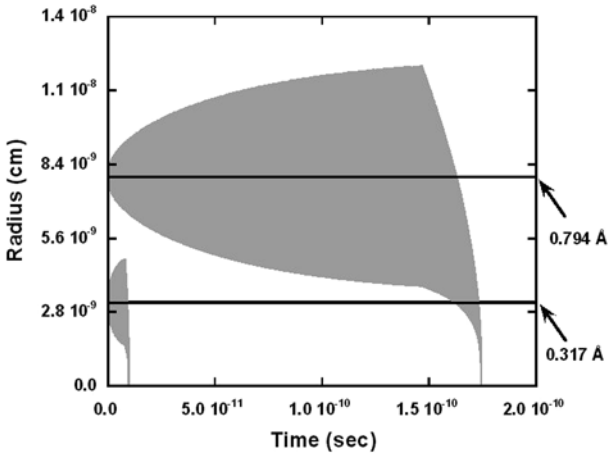

(d)

the full nonlinear differential equation solutions, and are in general fairly limited in their range of accuracy, as solving the full nonlinear equations seem in general to be necessary.

From (4) and (5), we will introduce the parameters

$$r = a_n + r', \tag{11}$$

and

$$\theta = \omega_n t + \theta', \tag{12}$$

where for the range of simulation we will examine here, we will assume that $|r'| \ll a_n$, and that $|\dot{\theta}'| \ll \omega_n$, which means that this expansion will only treat the early time evolution, such as in Fig. 3(c) and 3(d), where $|r'/a_n|$ and $|\dot{\theta}'/\omega_n|$ are still small, as opposed to the large envelope cases where clearly $|r'|$ can be an appreciable fraction of a_n, as in Fig. 1(a).

Fig. 4 (*Continued*)

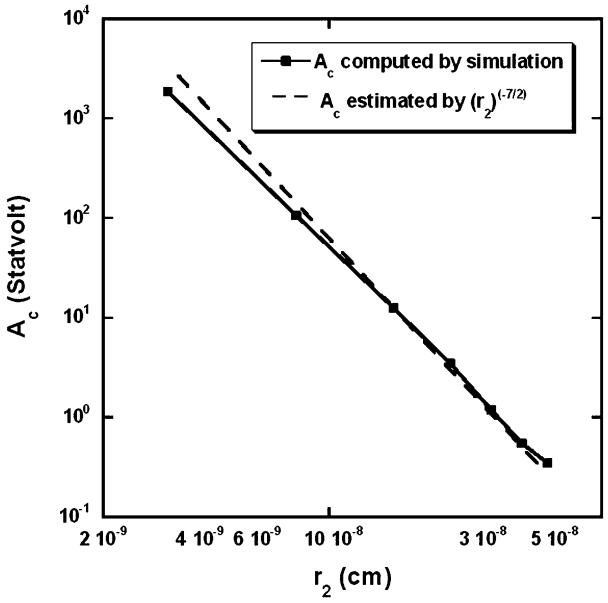

(e)

The present perturbation method will certainly shed some insight into the origin of such resonance conditions, however.

Equations (4) and (5) then become:

$$\ddot{r}' - (a_n + r')(\omega_n + \dot{\theta}')^2 = -\frac{e^2}{m(a_n + r')^2} + \frac{2\tau e^2}{m}\frac{\dot{r}'}{(a_n + r')^3} - \frac{eA}{m}\sin\big[(\omega_1 - \omega_n)t - \theta' + \alpha\big], \tag{13}$$

and

$$(a_n + r')\ddot{\theta}' + 2\dot{r}'(\omega_n + \dot{\theta}') = -\frac{\tau e^2}{m}\frac{(\omega_n + \dot{\theta}')}{(a_n + r')^2} + \frac{eA}{m}\cos\big[(\omega_1 - \omega_n)t - \theta' + \alpha\big]. \tag{14}$$

The Coulombic term in (13) can be expanded as:

$$\frac{e^2}{ma_n^2(1 + \frac{r'}{a_n})^2} = \frac{e^2}{ma_n^2}\left\{1 - 2\frac{r'}{a_n} + 3\left(\frac{r'}{a_n}\right)^2 - 4\left(\frac{r'}{a_n}\right)^3 + O\left[\left(\frac{r'}{a_n}\right)^4\right]\right\}. \tag{15}$$

As a first approximation, where we linearize all terms to first order in r', $\dot{r}'$, $\ddot{r}'$, $\dot{\theta}'$, and $\ddot{\theta}'$, and assuming products of these terms to be of second order in size, then yields:

$$\ddot{r}' - a_n\omega_n^2 - 2a_n\omega_n\dot{\theta}' - r'\omega_n^2 \approx -\frac{e^2}{ma_n^2} + 2\frac{e^2}{ma_n^2}\frac{r'}{a_n} + \frac{2\tau e^2\dot{r}'}{ma_n^3} - \frac{eA}{m}\sin\big[(\omega_1 - \omega_n)t - \theta' + \alpha\big], \tag{16}$$

and

$$a_n\ddot{\theta}' + 2\dot{r}'\omega_n \approx -\frac{\tau e^2}{m}\left(\frac{\omega_n}{a_n^2} + \frac{\dot{\theta}'}{a_n^2} - \frac{2\omega_n}{a_n^3}r'\right) + \frac{eA}{m}\cos\big[(\omega_1-\omega_n)t - \theta' + \alpha\big]. \tag{17}$$

It turns out, that because the radiation damping term is so extremely small, that only retaining the larger term of $\frac{\omega_n}{a_n^2}$ in (17) and dropping $\frac{\dot{\theta}'}{a_n^2}$ and $-\frac{2\omega_n}{a_n^3}r'$, is a fine approximation, at least for A not too large. Moreover, for up to several hundred orbits, θ' in the sine and cosine terms on the right sides of (16) and (17) remains quite small and can also be ignored. Also, in (16), we can identify that $a_n\omega_n^2 = \frac{e^2}{ma_n^2}$. The linearized equations then become:

$$\ddot{r}' - 2a_n\omega_n\dot{\theta}' - r'\omega_n^2 \approx +2\omega_n^2 r' + 2\tau\omega_n^2\dot{r}' - \frac{eA}{m}\sin\big[(\omega_1-\omega_n)t + \alpha\big], \tag{18}$$

and

$$\ddot{\theta}' + 2\frac{\dot{r}'}{a_n}\omega_n \approx -\tau\omega_n^3 + \frac{eA}{ma_n}\cos\big[(\omega_1-\omega_n)t + \alpha\big]. \tag{19}$$

Equation (19) can be integrated once, imposing the initial conditions that we will assume here that $\theta'(t=0)=0$, $\dot{\theta}'(t=0)=0$, $r'(t=0)=0$, and $\dot{r}'(t=0)=0$. We obtain that

$$\dot{\theta}' = -2\frac{r'}{a_n}\omega_n - \tau\omega_n^3 t + \frac{eA}{ma_n(\omega_1-\omega_n)}\{\sin[(\omega_1-\omega_n)t+\alpha] - \sin\alpha\}. \tag{20}$$

Substituting this back into (18) then results in a linearized 1D oscillator equation in terms of r':

$$\ddot{r}' - 2\tau\omega_n^2\dot{r}' + \omega_n^2 r' = -2\tau a_n\omega_n^4 t + \frac{eA}{m}\left\{\frac{(3\omega_n-\omega_1)}{(\omega_1-\omega_n)}\sin[(\omega_1-\omega_n)t+\alpha] - \frac{2\omega_n}{(\omega_1-\omega_n)}\sin\alpha\right\}. \tag{21}$$

Several cases of interest can immediately be recognized from this equation. If $n=2$, so that $\omega_1 = 2\omega_2$, then a secular situation arises when we neglect damping, since in the argument of the sine term, $(\omega_1-\omega_2)=\omega_2$, thereby providing a harmonic driving term of the same frequency as the resonant frequency of the oscillator equation. Initially ignoring the damping term (we'll correct this shortly), due to the very small value of $\tau = \frac{2}{3}\frac{e^2}{mc^3} \approx 6.266\times10^{-24}$ s for the classical electron, the above equation then becomes, for $n=2$,

$$\ddot{r}'_{\rm nd} \approx -\omega_2^2 r'_{\rm nd} + \frac{eA}{m}[\sin(\omega_2 t+\alpha) - 2\sin\alpha], \tag{22}$$

where the subscript "nd" indicates the no damping condition ($\tau=0$). Thus, the driving term acts at the resonant frequency, ω_2, of the oscillator equation. The solution to (22) is:

$$r'_{\rm nd}(t) = \frac{eA}{m(\omega_2)^2}\left\{2\sin\alpha[\cos(\omega_2 t)-1] + \frac{1}{2}\sin(\omega_2 t)\cos(\alpha) - \frac{t\omega_2}{2}\cos(\omega_2 t+\alpha)\right\}, \tag{23}$$

thereby revealing the secular term $t\frac{eA}{2m\omega_2}\cos(\omega_2 t)$ that grows without bound for this linearized equation of motion. The above result reveals an interesting feature of the $\omega/2$ subharmonic resonance; the linearized perturbation equations immediately involve a secular

situation. The same is true for $\dot{\theta}'$, which upon substituting (23) into (20) yields

$$\dot{\theta}'_{\rm nd} = \frac{eA}{ma_2\omega_2}\big\{t\omega_2\cos(\omega_2 t+\alpha)+3\sin\alpha-4\sin(\alpha)\cos(\omega_2 t) - \sin(\omega_2 t)\cos(\alpha)+\sin(\omega_2 t+\alpha)\big\}. \tag{24}$$

Integrating yields:

$$\theta'_{\rm nd} = \frac{eA}{ma_2(\omega_2)^2}[t\omega_2\sin(\omega_2 t+\alpha)+3t\omega_2\sin(\alpha) - 4\sin(\alpha)\sin(\omega_2 t)+\cos(\omega_2 t)\cos\alpha-\cos\alpha], \tag{25}$$

again revealing the secularly increasing harmonic terms.

For relatively small values of A, these solutions agree fairly well with the full numerical solution of (4) and (5) for the $n=2$ case, through the first few hundred orbits, as well as with the linearized case with damping included, from (20) and (21). Turning now to solve (20) and (21) with the damping correction, as well as for the general nth subharmonic case, yields

$$r'(t) = e^{\tau\omega_n^2 t}[a\cos(\omega t)+b\sin(\omega t)]_{\omega=\omega_n\sqrt{1-(\omega_n\tau)^2}} + r_{\rm p1}(t)+r_{\rm p2}+r_{\rm p3}(t), \tag{26}$$

where

$$r_{\rm p1}(t) \equiv \frac{eA}{m}\frac{(3\omega_n-\omega_1)}{(\omega_1-\omega_n)}\,{\rm Im}\left[\frac{e^{i[(\omega_1-\omega_n)t+\alpha]}}{-(\omega_1-\omega_n)^2-2\tau\omega_n^2 i(\omega_1-\omega_n)+\omega_n^2}\right], \tag{27}$$

$$r_{\rm p2} \equiv -\frac{2eA}{m\omega_n(\omega_1-\omega_n)}\sin\alpha, \tag{28}$$

$$r_{\rm p3}(t) \equiv -4\tau^2 a_n\omega_n^2 - 2\tau a_n\omega_n^2 t \tag{29}$$

and where a and b are given by

$$a = -r_{\rm p1}(0)-r_{\rm p2}-r_{\rm p3}(0), \tag{30}$$

$$b = -\frac{[\tau\omega_n^2 a+\dot{r}_{\rm p1}(0)+\dot{r}_{\rm p3}(0)]}{\omega_n\sqrt{1-(\omega_n\tau)^2}}, \tag{31}$$

in order to satisfy $r'(0)=0$ and $\dot{r}'(0)=0$. These solutions hold fairly well provided t is restricted to the $\tau\omega_n^2 t=(\omega_n\tau)(\omega_n t)\ll 1$ domain, due to $\omega_n\tau$ being so very small for atomic frequencies of interest, so that $e^{\tau\omega_n^2 t}\approx 1+\tau\omega_n^2 t$. In this case, the $-2\tau a_n\omega_n^2 t$ term from $r_{\rm p3}(t)$ combines with the secularly increasing $\tau\omega_n^2 t[a\cos(\omega t)+b\sin(\omega t)]$ term from (26), so that the radius decreases on average, in an oscillatory manner. (In particular, see Figs. 5(c) and 5(d), to clarify the meaning of this last statement.)

Figures 5(a) and 5(b) below show these comparisons for the specific case where $r_1 = 0.5$ Å, or, $r_2 = 0.5\times 2^{2/3}$ Å ≈ 0.7937 Å. In Fig. 5(a), with $A=106$ Å, $n=2$, there are three curves superimposed, one being the full nonlinear numerical solutions to (4) and (5), the second being (23), where damping was not included, and the third being the linearized solution with damping included, (26). As can be seen in Fig. 5(a), up through $t=10^{-14}$ s, the solutions lie fairly much on top of each other, with only slight differences that can be

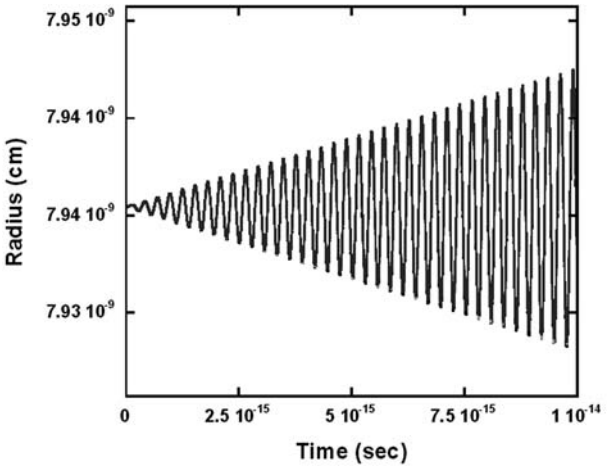

(a)

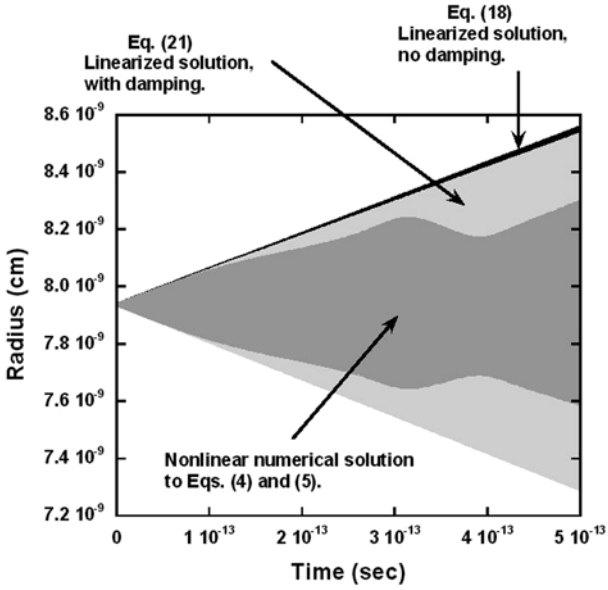

(b)

Fig. 5 For (**a**) and (**b**), $r_1 = 0.5$ Å, $r_2 = 0.5 \times 2^{2/3}$ Å ≈ 0.7937 Å, $A = 106$ Å, $n = 2$, $\alpha = 0$. (**a**) $r'(t) + a_2$ vs. t, using the full nonlinear solutions to (4) and (5), as well as the linear solution without damping, namely, (18), and finally the linear solution with damping included, (21). The three solutions lie fairly much on top of each other for the short time period shown. (**b**) The same conditions are simulated here as in (**a**), but the time is taken out farther to 5×10^{-13} s. Now a clear difference in the solutions can be seen. Note that the "linearized solution, no damping" curve lies behind the other two, and only the top edge is visible here. However, the envelope of this curve is essentially as "wide" and of the same shape as the "linearized solution, with damping" curve, but it (*the dark curve*) does not slowly decay. Hence, the top edge of it is visible here, while the bottom edge is covered by the slowly decaying (*lightly colored*) envelope. (**c**) $r'(t) + a_3$ vs. t, for $n = 3$, $\alpha = 0$. The approximate analytic solution of (26) and the numerical solution to (4) and (5) are superimposed here for $A = 100$ statvolt/cm and $A = 500$ statvolt/cm. The solutions lie virtually on top of each other, as they are nearly independent of A. (**d**) $r'(t) + a_4$ vs. t, for $n = 4$, $\alpha = 0$. The approximate analytic solution and full numerical solution are virtually indistinguishable, for both the $A = 100$ statvolt/cm and $A = 500$ statvolt/cm conditions, although the 100 vs. 500 curves are clearly distinguishable

Fig. 5 (*Continued*)

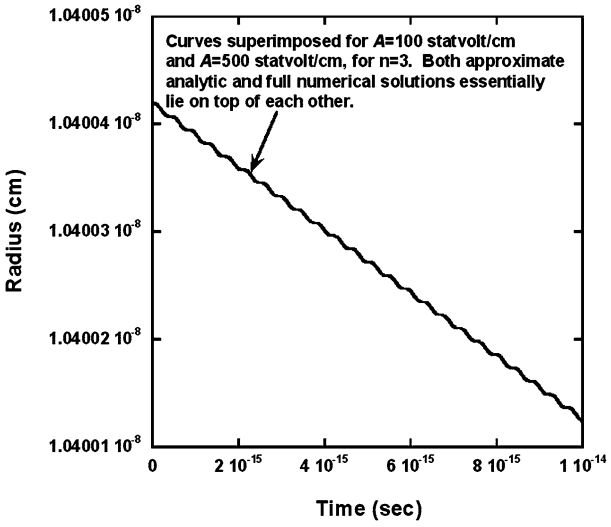

(c)

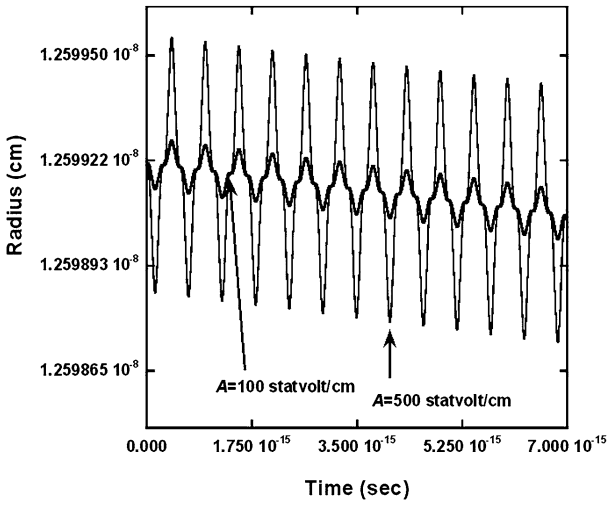

(d)

seen if one zooms in on the peaks and valleys. However, when going out further in time, as in Fig. 5(b), then substantial differences occur, as should be expected. The "beat" like pattern of the envelope (i.e., the envelope oscillating in and out), occurs from the nonlinear solution, but is not evident in the linear solutions. Also, when damping is included in the linear solution, one sees the slow decay of the orbit taking place. If we were to show similar plots for $\theta'(t)$, very analogous results would be seen. Our linear solutions with and without damping follow the full nonlinear numerical solutions for the early time development, but eventually are not able to predict the nonlinear changes that unfold. Similar situations hold for any value of n, where so long as $|r'| \ll a_n$, then reasonable results are predicted from the linearized equations, as should be expected. Thus, if we examine larger values of A, the linearized equations are reasonable approximations for shorter periods of time.

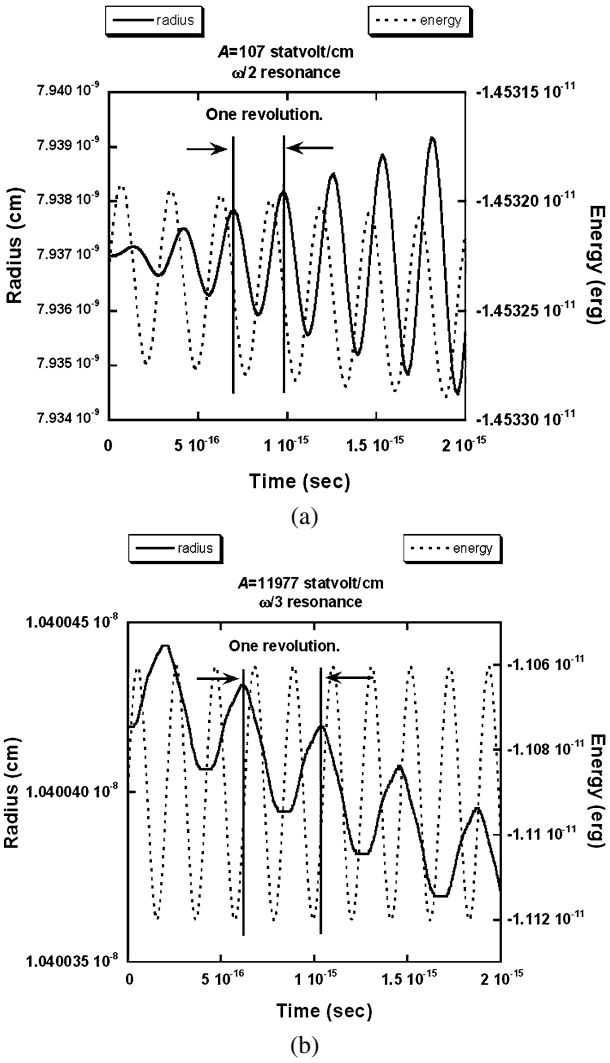

Fig. 6 (**a**) $r'(t) + a_2$ vs. t for $n = 2$, $\alpha = 0$, $A = 106$ statvolt/cm, as well as $E = \frac{m\mathbf{v}^2}{2} - \frac{e^2}{r}$ vs. t are plotted. (**b**) $r'(t) + a_3$ vs. t for $n = 3$, $\alpha = 0$, $A = 11,977$ statvolt/cm, as well as $E = \frac{m\mathbf{v}^2}{2} - \frac{e^2}{r}$ vs. t are plotted. (**c**) $r'(t) + a_4$ vs. t for $n = 4$, $\alpha = 0$, $A = 147{,}087$ statvolt/cm, as well as $E = \frac{m\mathbf{v}^2}{2} - \frac{e^2}{r}$ vs. t are plotted. The period of each orbit, namely, $\frac{2\pi}{\omega_n}$, increases linearly with n, as can be visually seen in the plots, since $\omega_n = \omega_1/n$, so the period is given by $T_n = \frac{2\pi}{\omega_n} = \frac{2\pi}{\omega_1} n$

What is also interesting here is to consider the $n = 3$ case, since here $(3\omega_n - \omega_1) = 0$, so $r_{\mathrm{p1}}(t) = 0$, thereby removing a strong component of the dependence of $r'(t)$ on the amplitude A of the CP plane wave. Indeed, when $\alpha = 0$ and $n = 3$, then the approximate analytic prediction of (26) predicts that $a = 4\tau^2 a_n \omega_n^2$, $b \approx 2\tau a_n \omega_n$, and, with $\omega_n \tau \ll 1$,

$$r'(t) \approx e^{\tau\omega_n^2 t}\left[4\tau^2 a_3 \omega_3^2 \cos(\omega_3 t) + 2\tau a_3 \omega_3 \sin(\omega_3 t)\right] - 4\tau^2 a_3 \omega_3^2 - 2\tau a_3 \omega_3^2 t,$$

so that $r'(t)$ is virtually independent of A. This is confirmed by Fig. 5(c), which shows the approximate analytic solution versus the full numerical solution from (4) and (5), for the cases when $A = 100$ statvolt/cm and $A = 500$ statvolt/cm. All four curves essentially lie on top of each other in Fig. 5(c). Of course, if A becomes much larger, then the nonlinear terms ignored earlier become increasingly more important, thereby causing $r'(t)$ to again depend strongly on the value of A, as can be seen in the numerical experiments of Fig. 3.

Fig. 6 (*Continued*)

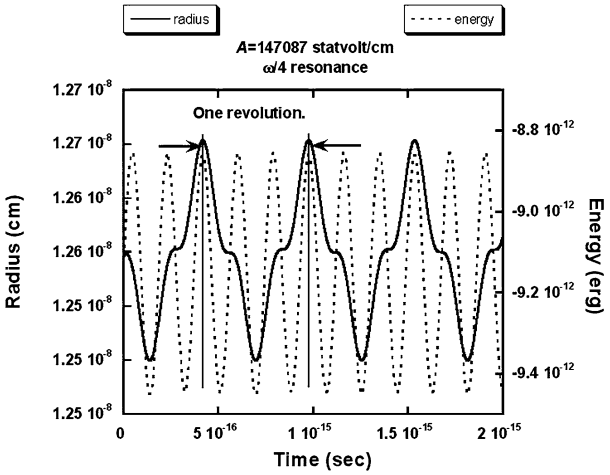

(c)

Figure 5(d) shows the analogous case for $n = 4$, $\alpha = 0$. In contrast with the $n = 3$ solutions, the $n = 4$ solutions are again heavily dependent on the value of A. Figure 5(d) shows the approximate analytic curve, and the full numerical solution curve, for two cases, namely, where $A = 100$ statvolt/cm and $A = 500$ statvolt/cm. The approximate analytic curve and the full numerical solution are virtually indistinguishable. Only if we carry these simulations farther out in time, as was done in Fig. 5(b) for the $n = 2$ case, will differences be seen.

4 Simulation Study on the Approach to Resonance

Let us now discuss the physical origin of the subharmonic resonances that have been illustrated here. When the period of the orbit of the classical charged particle is a multiple of the period of the acting CP plane wave, then to first order, in each orbit as much work is done on the orbiting particle by the CP plane wave as is done to retard the orbiting particle. If this was precisely the case, however, then a resonance condition would not be established, and the orbit of the particle would just tend to decay, due to the constantly acting damping effect of the radiation reaction term. However, the orbit is slightly perturbed by the CP plane wave, and often in just such a way that slightly more positive work is done per orbit by the CP plane wave, then negative work. This results in the resonance conditions seen so far. Exactly what values of A and α will ensure this result to occur is what makes the analysis so difficult, although, as we saw, when A is greater than certain critical values, dependent on the value of n, then resonance is likely to take place.

The kinetic plus potential energy,

$$E = \frac{m\mathbf{v}^2}{2} - \frac{e^2}{r}$$

versus time plots reveal additional insight into the dependence of resonance on the value of A. Here we show a few numerical examples. One needs to examine values of time sufficiently long to be able to recognize this dependence clearly. For example, Figs. 6(a), (b), and (c) show plots of $r(t)$ vs. t and E vs. t, for $n = 2, 3, 4$ respectively, with $\alpha = 0$, and A

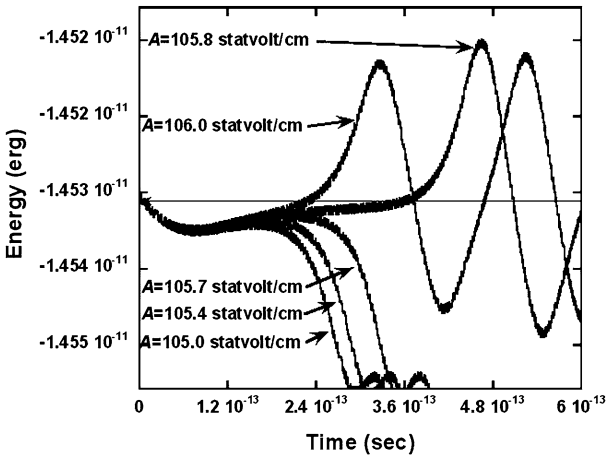

(a)

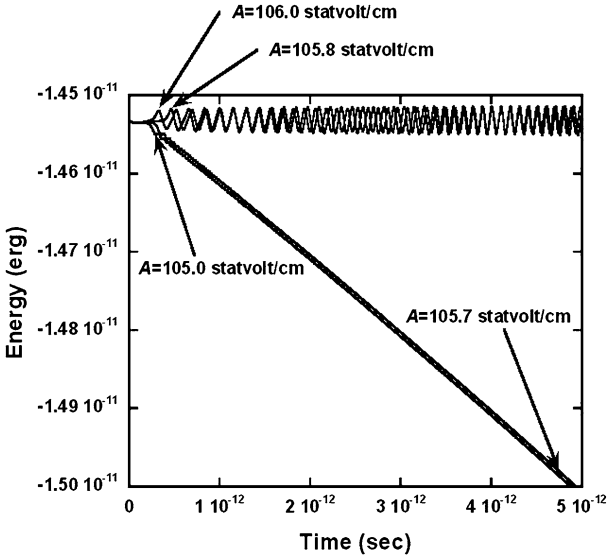

(b)

Fig. 7 (**a**) $E = \frac{mv^2}{2} - \frac{e^2}{r}$ vs. t for the classical charged particle starting in a circular orbit at $r = r_2 = 0.5\ \text{Å} \times 2^{2/3}$, with $\alpha = 0$, for several different values of A. Just a small change in A, near $A_c \approx 105.8$ statvolt/cm, can have significant effects on the delay to orbital decay. (**b**) E vs. t as in (**a**), but carried out farther in time. (**c**) r vs. t curves for conditions as in (**a**), but carried out farther in time. (**d**) A zoomed-in view of r vs. t for the conditions in (**c**), to illustrate how the inner behavior within the envelopes are quite different, although the period of the oscillations is nearly identical

chosen to be close to the critical value of A needed to establish resonance. For these plots, the linearized solutions obtained above agree well with the nonlinear expressions. In each of the three cases shown, a variation in E vs. t is observed, but the change in E is very small per orbit, namely, a fractional change in orbit of about 2×10^{-5} per orbit for the $n = 2$ case, 5×10^{-3} for the $n = 3$ case shown, and 7×10^{-2} for the $n = 4$ case. These fractions are larger as n increases, since much larger values of A are required to obtain resonance as n becomes larger (i.e., see Fig. 4(a)). Looking at each of these E vs. t plots, one might suspect that resonance really was not yet established, since in each case, the average of the E values tends to be decreasing, leading one to suspect orbital decay will occur.

However, looking at much longer time periods, very different insights can be gained. As the orbit decays, the relationship between the phase of the force from the CP plane wave to the velocity of the orbiting particle changes in subtle ways. Figure 7(a) illustrates this point,

Fig. 7 (*Continued*)

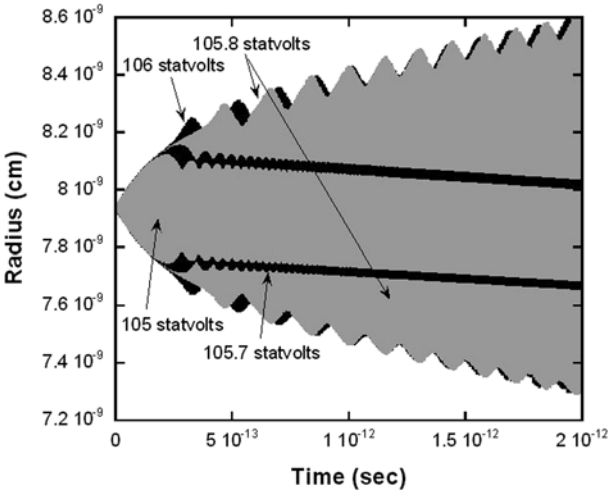

(c)

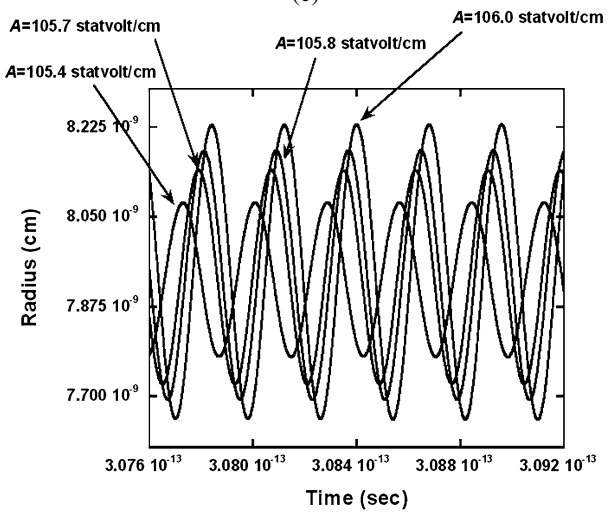

(d)

as when A is large enough, namely, greater than or equal to 105.8 statvolt/cm for the $n = 2$ case with $r_1 = 0.5$ Å, then the average value of E is able to increase sufficiently to again become larger than its starting value, which then results in a very long pattern of oscillating increases and decreases in E vs. t, very much remindful of the patterns found in the $\omega/1$ resonances in [1]. Figure 7(b) illustrates how far out in time this behavior continues; clearly, just a small change in A of as small as 0.1 statvolt/cm can have a dramatic change in the ensuing orbital trajectory. Figure 7(c) shows the associated r vs. t plot. The close similarity to Fig. 3(e) for the $\omega/3$ subharmonic resonant case should be noted.

To find the points of resonances in Figs. 4(a)–(d), plots of E vs. t similar to Fig. 7(a) were used, as these were the most sensitive to enable the detecting of the point of resonance. The general condition seemed to be that when E again returned and surpassed its original value, and when the point at which this occurred in time was as far out in time as possible, then the

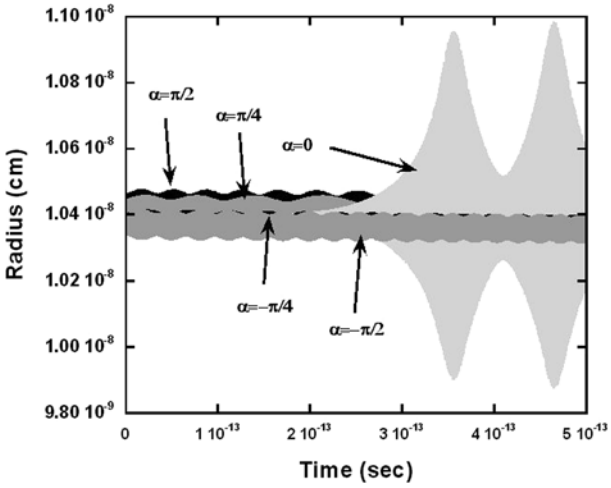

Fig. 8 r vs. t for the classical charged particle beginning in a circular orbit at $r = 3^{(2/3)} \times 0.5$ Å, with a CP plane wave of frequency ω_1 corresponding to the frequency of a circular orbit at 0.5 Å. $A = 13{,}000$ statvolt/cm. Each curve represents a different value of α used in the simulations, where α occurs in (4) and (5)

critical transition value of A could be defined. For A below this value, orbital decay would soon clearly occur, as in the $A \leq 105.7$ statvolt/cm cases in Fig. 7(a), and for A above this value, as in the $A \geq 105.8$ statvolt/cm cases in Fig. 7(a), oscillating values of E vs. t would continue for very long times about the initial value of E. It should be noted, however, that each of the E vs. t curves in Figs. 7(a) and 7(b) have a fine structure "wiggle" to them, if zoomed in upon, corresponding to the curves shown in Figs. 6(a)–(c), due to the oscillations in E during each revolution of the particle's orbit. Figure 7(c) shows the corresponding curves of r vs. t to the energy curve of Fig. 7(b). Clearly, the energy vs. t curves provide a clearer indication of a stability condition.

Figure 8 shows the effect of the parameter α on radius; this effect was studied in some detail in [3] and [4]. More specifically, in this earlier work, a strong dependence was found on making the classical electron stay in a resonant orbit, without decay, on both A and on α, where α is again the initial angle between the classical electron's velocity and the force $(-e)\mathbf{E}_{\mathrm{CP}}$ at time $t = 0$.

Figure 8 contains plots of r vs. t, for the $\omega/3$ subharmonic resonance condition, with $A = 13,000$ statvolt/cm, for various values of α, where in each case the classical charged particle was started in an initial circular orbit at $r_3 = 0.5 \times 3^{2/3}$ Å. The effect of α for the same value of A, largely does not appear to change the general condition of resonance, but displaces the point at which large versus small "beat-like" oscillations in the r vs. t envelope curve will take place, which in turn will strongly effect the point at which eventual orbital decay will take place, as in [3] and [4] for the $\omega/1$ case.

Finally, we note further effects of very large values of A on radius in Fig. 9. Here, $A = 80{,}000$ statvolt/cm and the $\omega/2$ resonance and stability conditions were examined. Three initial starting values of r are shown in Fig. 9(b); the same frequency for the applied circularly polarized plane wave is used for all curves, so the stable radial condition only holds for the initial $r = 0.5$ Å case. Only within a very narrow regime does the stability/resonant condition actually hold, namely, within a frequency range of about $\pm 0.3\%$ of the resonant frequency [4, 5], which would correspond here to a starting radius in the range of about ± 0.0015 Å around the 0.5 Å starting point. The point of the plots in Fig. 9(b) is to illustrate how wide the envelope of the r vs. t curves are with such a large value of A. However, even though there is near overlap of the envelopes, stability is clearly seen only for the $r = 0.5$ Å case.

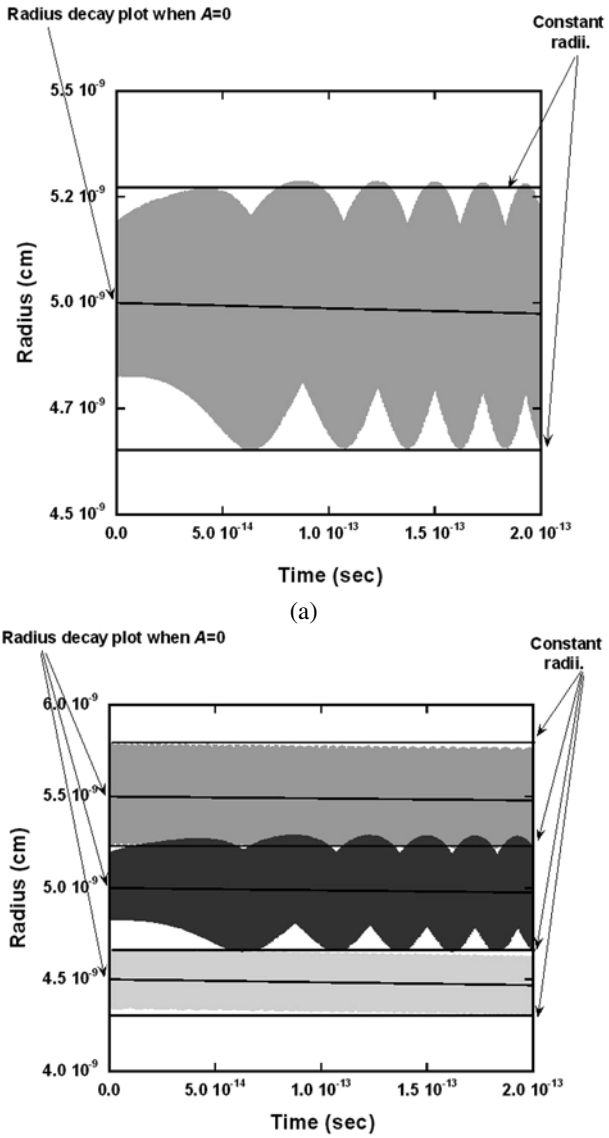

Fig. 9 r vs. t for the large A case of $A = 80{,}000$ statvolt/cm, for an $\omega/2$ resonance condition. As can be seen, the outer envelope remains fairly level, indicating the strong resonance condition even for this large A condition. (**a**) The initial radius is 0.5 Å. Also shown is the decay curve when $A = 0$. (**b**) Three initial values of r are shown, all under the $\omega/2$ resonance condition: $r = 0.55$ Å, 0.50 Å, and 0.45 Å. In each case the same frequency for the applied circularly polarized plane wave is used, so the resonant condition only holds for the initial $r = 0.5$ Å case. The center line of the three envelope curves in (**b**) correspond to the case where radial decay occurs due to $A = 0$. As can be seen, the envelopes of the $r = 0.55$ Å and $r = 0.45$ Å curves are decaying (they are nearly parallel to the $A = 0$ decaying curves), while the $r = 0.50$ Å curve does not

5 Concluding Remarks

In previous work, the effect of applying a CP plane wave to a classical electron in an initial circular orbit, when the angular frequency of the CP wave matched the angular frequency of the orbit, was described in some detail [1, 3, 4]. This study was extended to the case of elliptical orbits [2], where an infinite set of harmonic frequencies associated with the general periodic motion was needed to be considered. In all cases, very distinctive resonance conditions were obtained that could be modified by the amplitude of the CP wave and the phase of the CP wave in relation to the orbital motion of the classical electron. In

all cases, the initial circular and/or elliptic orbit was significantly altered as a result of the applied driving force, as might be expected, but with substantial delays in orbital decay occurring, which seemed difficult to anticipate to such an extent. Many of these effects have since been confirmed experimentally [10]. In future work, we hope to make more detailed comparisons.

The present article studied the case where subharmonic resonances took place for initially near circular orbits. In the situations studied here, the classical charge particle, following the nonrelativistic Lorentz-Dirac equation, was started in an initial circular orbit, with a CP plane wave acting with a frequency n times greater than the frequency of the orbiting particle. In this way, the CP wave acts nearly periodically, with roughly equal times of the orbital period, T, for the positive work versus the negative work done on the orbiting particle by the CP wave. However, the orbit is perturbed slightly, and when the amplitude of the CP wave A is larger than a critical value, then the orbit is perturbed in just such a way to make the amount of positive work by the CP wave, per orbit, equal on average to the energy radiated due to the radiation reaction.

A perturbation analysis was carried out that showed the origin of the resonance effects. This analysis showed the origin of secular resonance in the $n = 2$ case, and the near independence on A in the $n = 3$, $\alpha = 0$ cases. The perturbation analysis agreed well with full numerical solutions provided that A was not too large and that one did not go out too far in time, as then strong nonlinear effects enter that in general require the full numerical solution of the equations of motion. Examples of these resonance effects were shown in some detail.

To the best of our knowledge, such subharmonic resonance effects have not been reported elsewhere for the Coulombic binding potential. As shown here, the effects can be very dramatic, even more so than the interesting $\omega/1$ resonance effects discussed elsewhere. Just a very small change in A can make an enormous difference in the subsequent trajectory of the charged particle. We believe these effects should translate into similar effects for near elliptical orbits; and some studies have been carried out to date by us that indicates this is true. Finally, to what degree of importance these resonance effects might play in the general theory of SED [6, 7], or in the case of experimental results for strong applied fields to the hydrogen or Rydberg atoms, remains to be seen. We do note that there seems to be some striking experimental evidence regarding the ratio of a driving microwave frequency to the classical Kepler frequency of Rydberg atomic systems, and the effects of such ratios on the ionization, and stabilization, of such atomic systems [8, 9].

The work described here contained considerable reliance on simulation, as analytic solutions to the very nonlinear equations of motion are not known. However, to provide greater confidence in these results, most were carried out with several levels of numerical precision, plus with simulations based on the $x - y$ equations of motion, and the $r - \theta$ equation of motion emphasized in this article. In addition, semianalytic analyses were carried out and reported here to help understand the simulation results.

Since the work in this article was completed, further analysis has revealed deeper understanding in the evolution of the approximate semimajor axis, the semiminor axis, the ellipticity, the energy, and the angular momentum, during periods of subharmonic resonance. Such results will be reported in future work.

Finally, we note that the simple tests we have carried out do not readily reveal the observance of harmonic resonances of the form $n\omega_1$ (i.e., superharmonic resonances), or of the form $\frac{n\omega_1}{m}$, where n and m are integers. Such resonances may still be present, if α and A are of the right values, but our strong impression is that these resonances, if they exist, are of a much less pronounced character than the subharmonic resonances reported here.

References

1. Cole, D.C., Zou, Y.: Simulation study of aspects of the classical hydrogen atom interacting with electromagnetic radiation: Circular orbits. J. Sci. Comput. **20**(1), 43–68 (2004)
2. Cole, D.C., Zou, Y.: Simulation study of aspects of the classical hydrogen atom interacting with electromagnetic radiation: Elliptical orbits. J. Sci. Comput. **20**(3), 379–404 (2004). Preprint available at http://www.bu.edu/simulation/publications/dcole/publications.html
3. Cole, D.C., Zou, Y.: Perturbation analysis and simulation study of the effects of phase on the classical hydrogen atom interacting with circularly polarized electromagnetic radiation. J. Sci. Comput. **21**(2), 145–172 (2004). Preprint available at http://www.bu.edu/simulation/publications/dcole/publications.html
4. Cole, D.C., Zou, Y.: Analysis of orbital decay time for the classical hydrogen atom interacting with circularly polarized electromagnetic radiation. Phys. Rev. E **69**(1), 16601 (2004)
5. Cole, D.C., Zou, Y.: Quantum mechanical ground state of hydrogen obtained from classical electrodynamics. Phys. Lett. A **317**(1–2), 14–20 (2003)
6. de la Peña, L., Cetto, A.M.: The Quantum Dice—An Introduction to Stochastic Electrodynamics. Kluwer Academic, Dordrecht (1996)
7. Cole, D.C.: Reviewing and extending some recent work on stochastic electrodynamics. In: Lakhtakia, A. (ed.) Essays on the Formal Aspects of Electromagnetic Theory, pp. 501–532. World Scientific, Singapore (1993)
8. Noel, M.W., Griffith, W.M., Gallagher, T.F.: Classical subharmonic resonances in microwave ionization of lithium Rydberg atoms. Phys. Rev. A **62**, 063401 (2000)
9. Koch, P.M., van Leeuwen, K.A.H.: The importance of resonances in microwave "ionization" of excited hydrogen atoms. Phys. Rep. **255**, 289–403 (1995)
10. Maeda, H., Norum, D.V.L., Gallagher, T.F.: Microwave manipulation of an atomic electron in a classical orbit. Science **307**, 1757–1760 (2005)
11. Teitelboim, C., Villarroel, D., van Weert, Ch.G.: Classical electrodynamics of retarded fields and point particles. Riv. Nuovo Cim. **3**(9), 1–64 (1980)
12. Boyer, T.H.: Random electrodynamics: The theory of classical electrodynamics with classical electromagnetic zero–point radiation. Phys. Rev. D **11**(4), 790–808 (1975)
13. Cole, D.C.: Derivation of the classical electromagnetic zero–point radiation spectrum via a classical thermodynamic operation involving van der Waals forces. Phys. Rev. A **42**, 1847–1862 (1990)
14. Cole, D.C.: Reinvestigation of the thermodynamics of blackbody radiation via classical physics. Phys. Rev. A **45**, 8471–8489 (1992)
15. Nayfeh, A.H., Mook, D.T.: Nonlinear Oscillations. Wiley, New York (1979)
16. Press, W.H., Teukolsky, S.A., Vetterling, W.T., Flannery, B.P.: Numerical Recipes: The Art of Scientific Computing, 3rd edn. Cambridge University Press, Cambridge (2007)